Microporous and Mesoporous Materials 325 (2021) 111314

Contents lists available at ScienceDirect

Microporous and Mesoporous Materials

journal homepage: www.elsevier.com/locate/micromeso

The joint effect of naphthalene-system and defects on dye removal by UiO-66 derivatives

Vera V. Butova [a,*], Abdelaziz M. Aboraia [a,b], Malak Solayman [a], I.S. Yahia [c,d], Heba Y. Zahran [c,d], Alaa F. Abd El-Rehim [c,d], Hamed Algarni [c], Gomaa Khabiri [e], Alexander V. Soldatov [a]

[a] Smart Materials Research Institute, Southern Federal University, Sladkova 178/24, 344090, Rostov-on-Don, Russia
[b] Department of Physics, Faculty of Science, Al-Azhar University, Assiut, 71542, Egypt
[c] Advanced Functional Materials & Optoelectronic Laboratory, Department of Physics, Faculty of Science, King Khalid University, P.O. Box 9004, Abha, Saudi Arabia
[d] Nanoscience Laboratory for Environmental and Bio-medical Applications (NLEBA), Semiconductor Lab., Department of Physics, Faculty of Education, Ain Shams University, Roxy, 11757, Cairo, Egypt
[e] Physics Department, Faculty of Science, Fayoum University, Fayoum, 63514, Egypt

ARTICLE INFO

Keywords:
MOF
Photocatalysis
Naphthalene
Methylene blue
Products of degradation
Oxidative demethylation

ABSTRACT

We report the results of the application of UiO-66 derivates for dye removal. This complex process includes two parallel mechanisms. The first one is the adsorption of the dye into the pores of MOF. The second one is photocatalytic degradation. We used two linkers for MOF synthesis: 1,4-benzene dicarboxylate and 1,4-naphthalene dicarboxylate. The introduction of these molecules in various ratios into the UiO-66-type structure allowed us to trace the effect of naphthalene species on the methylene blue removal. It was shown that a conjugated π-system of naphthalene rings led to charge transfer from linker to zirconium ions. It reduces the bandgap of the material and, therefore, results in higher photocatalytic performance. We also traced the effect of defects in the MOF structure on methylene blue degradation. It was shown that unsaturated zirconium ions in defect pores effectively catalyze dye cleavage and direct this process to the oxidative demethylation pathway. Obtained results could be applied to improve the photocatalytic properties of UiO-66 derivates.

1. Introduction

In the last decades, many researchers attempt to solve the issue of pollutants in different ways. One of these routes is photocatalysis via conversion of the contaminant to water (H_2O) and carbon dioxide (CO_2) [1–5]. Metal oxide semiconductor materials, such as titanium dioxide, zirconium oxide, zinc oxide et al. were utilized as photocatalysts to remove environmental pollutants [6–12]. However, two significant problems reduce those further applications. The photo-induced electron-hole (*e-h*) pairs readily rapid recombination leads to a decrease of photocatalytic efficiency. Also, the response to visible light is often poor, and the *e-h* pairs are stimulated by ultraviolet (UV) light. Several attempts have been reported to overcome these issues. However, the preparation of new efficient and eco-friendly photocatalysts is a significant challenge [13–15].

The metal-organic frameworks (MOFs) are a new generation of porous crystal materials consisting of organic linkers and inorganic secondary building units (SBU). MOFs were applied in several fields, such as gas storage and separation, catalysis, molecular sensing, drug delivery and others [16–23]. Recently MOFs were also applied for photocatalytic degradation of pollutants [24,25]. The common mechanism of photochemical reaction includes photoexcitation of electrons from HOMO to LUMO with h^+ simultaneous formation. This metastable state results in interaction with water and the production of active •OH radicals, which could effectively cleave dyes [26–28]. It was also shown that charge transfer from conjugated π-system of benzene rings to metallic sites in SBUs could reduce bandgap and enhance the photocatalytic performance [29,30].

UiO-66 is one of the MOFs, which attracts a lot of attention due to its stability and high porosity. It consists of Zr-ions and 1,4-benzene dicarboxylate linkers. Each SBU contains six zirconium ions and is coordinated by twelve linkers. UiO-66 and its derivates were successfully applied for selective adsorption of dyes [31–34]. UiO-66-type MOFs could contain a lot of defects, such as missing linkers or even missing SBUs. Zirconium ions in the defect pores are coordinated by temporary monodentate ligands instead of bidentate linkers. Washing and

* Corresponding author.
E-mail address: vbutova@sfedu.ru (V.V. Butova).

https://doi.org/10.1016/j.micromeso.2021.111314
Received 30 April 2021; Received in revised form 6 July 2021; Accepted 19 July 2021
Available online 23 July 2021

activation procedures lead to the formation of Zr-unsaturated sites, which exhibit high catalytic activity [35,36].

In the present work, we have used methylene blue (MB) as a model contaminant to trace its photocatalytic degradation under visible light in the presence of UiO-66-type MOFs. We used materials with two linkers (1,4-benzene dicarboxylate (BDC) and 1,4-naphthalene dicarboxylate (NDC)) in various ratios in one phase. It allowed us to trace the effect of the naphthalene π-system on the decomposition process. We also synthesized analogs of these MOFs with high defect concentrations. These materials were compared to evaluate the impact of unsaturated zirconium sites on MB degradation.

2. Experimental

2.1. Synthesis

Zirconium tetrachloride, 1,4-naphthalene dicarboxylic acid (H_2NDC), terephthalic acid (H_2BDC), benzoic acid (BA), N, N-dimethylformamide (DMF), isopropanol, methylene blue (MB) were purchased from Alfa Aesar and used without further purification. Deionized (DI) water (18 MΩcm) was obtained from a Simplicity UV ultrapure water system.

MOF samples were synthesized according to the reported technique [37,38] (Fig. 1). Briefly, zirconium tetrachloride was dissolved in DMF, and water was dropped into the reaction mixture. We then added the respective linker or their combination, waited for their complete dissolution, and placed a clear colorless solution into the preheated oven for crystallization at 120 °C for 24 h. We have added BA after water before linkers to synthesize 100BDC0NDC-60, 75BDC25NDC-60, 50BDC50NDC-60 samples. The rest of the technique was the same. Used masses and volumes of precursors are provided in Table 1. After 24 h of heating, white precipitates were formed on the bottom of the vessel. They were cooled down to room temperature, separated via centrifugation, and washed twice with DMF and twice with isopropanol. Finally, samples were dried at 60 °C for 12 h.

2.2. Catalytic tests

For the catalytic performance, we used MB solution in water with a concentration of 10 mg per liter. A respective sample (25 mg) was placed into 50 ml of the MB solution and mixed using a magnetic stirrer. One part of the suspension was kept in the dark place under constant stirring.

Table 1
vol and weights of used precursors.

Sample designation	Weights of precursors, g				Volumes of precursors, ml	
	$ZrCl_4$	BDC	NDC	BA	DMF	Water
100BDC0NDC	0.5042	0.3591	0	0	50	0.1167
75BDC25NDC		0.2693	0.1168			
50BDC50NDC		0.1796	0.2337			
0BDC100NDC		0	0.4673			
100BDC0NDC-60	0.5042	0.3591	0	15.8393	50	0.1167
75BDC25NDC-60		0.2693	0.1168			
50BDC50NDC-60		0.1796	0.2337			

These solutions are designated as “dark” in text. Another part was magnetically stirred for 30 min in the dark place with subsequent irradiation with white light at room temperature. These solutions are designated as “light” further in the text.

We have taken probes of the suspensions at regular intervals, separated clear solutions via centrifugation, and analyzed it using UV–Vis spectrometer to trace MB concentration.

2.3. Methods

Bruker D2 PHASER X-ray diffractometer (CuK_α, $\lambda = 1.5417$ Å) was used to record powder XRD patterns with a step of 0.01°. The analysis of diffraction patterns was done in FullProf software. Nitrogen adsorption/desorption isotherms were measured on Accelerated Surface Area and Porosimetry analyzer ASAP 2020 (Micromeritics) at −196 °C. The samples were activated under a dynamic vacuum at 150 °C for 12 h before the measurement. Specific surface areas were calculated according to the BET model. Pore size distribution was calculated by Non-Local Density Functional Theory according to the Tarazona model of cylindrical pores. IR spectra were recorded on a Bruker Vertex 70 spectrometer in ATR geometry (Attenuated total reflectance) using an MCT detector and a Bruker Platinum ATR attachment. The spectra were measured in the range from 5000 to 30 cm^{-1} with a resolution of 1 cm^{-1} and 64 scans. The reference was air. UV–Vis spectra were collected on UV-2600 (Shimadzu) spectrophotometer.

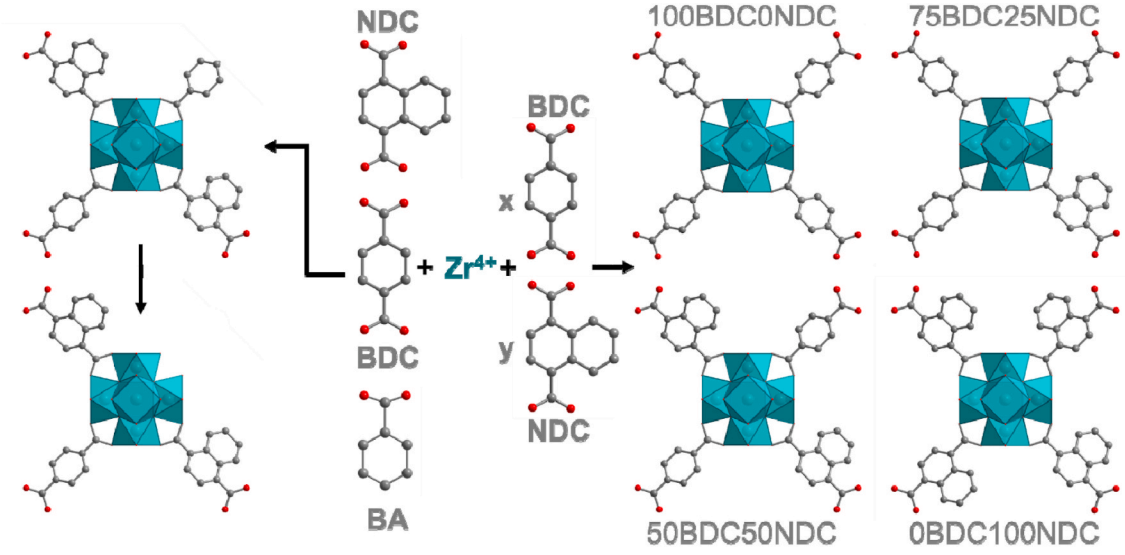

Fig. 1. Schematic representation of the MOFs’ synthesis. The right part demonstrates the production of UiO-66-type MOFs with a mixture of two linkers – BDC and NDC. The left part shows the introduction of BA for defect formation.

3. Result and discussion

3.1. MOFs

XRD profiles are presented in SI Fig.S 1. All as-prepared samples possess a UiO-66 structure with cubic symmetry (Table 2). The lattice parameters increased with an increase in NDC content. It could be attributed to the stress created by extra benzene rings of the NDC linker in comparison with the BDC ligands in good agreement with previously reported data [37].

FTIR spectra of synthesized materials are provided in Fig. 2a. Observed modes are in good agreement with the linker composition of the synthesized sample. Particularly, sample 100BDC0NDC contains a terephthalate linker, so its spectrum contains characteristic modes at 745, 1020, 1395 cm^{-1} (highlighted with gray dotted lines in Fig. 2a). The peak at 745 cm^{-1} could be assigned to C-H wagging in-plane, while one at 1395 cm^{-1} could be attributed to symmetric stretching of O-C-O carboxylic group [37]. Conversely, the 0BDC100NDC sample contains only 1,4-naphthalene dicarboxylate linker, and its spectrum exhibits its characteristic peaks: 790, 1170, 1215, 1267, 1365, 1460 cm^{-1} (highlighted with green dashed lines in Fig. 2a). The peak at 790 cm^{-1} corresponds to C-H in-plane wagging [37]. C-C skeletal vibrations and deformation vibrations of naphthalene rings give rise to peaks at 1170 and 1215 cm^{-1}, respectively [39]. Peaks at 1267, 1365, and 1460 cm^{-1} could be attributed to C-H out-of-plane banding and C-C stretching [37]. Fig. 2b represents nitrogen sorption isotherms of samples 0BDC100NDC, 50BDC50NDC, 75BDC25NDC and 100BDC0NDC. All of them exhibit the same shape, which could be attributed to type I according to IUPAC notifications. It indicates the microporous nature of these MOFs. Specific surface areas of the samples increase with a decrease of NDC content (Table 2). This trend is attributed to extra space in the pore, which is required by the naphthalene ring of NDC-linker compared to one benzene ring of BDC-linker.

Samples 100BDC0NDC-60, 75BDC25NDC-60, and 50BDC50NDC-60 exhibit a similar structure with UiO-66 according to XRD (Fig. S2 in SI). FTIR spectra of these samples contain peaks in good agreement with linker composition (Fig. 3a). It should be highlighted that an additional peak at 717 cm^{-1} could be assigned to benzoic acid, and it was not observed on spectra of samples obtained without BA additive (these peaks are highlighted with a blue dashed line in Fig. 3a). Fig. 3b represents nitrogen sorption isotherms of samples 100BDC0NDC-60, 75BDC25NDC-60, and 50BDC50NDC-60. All of them correspond to type I according to IUPAC notifications, as well as MOFs synthesized without BA additive. However, samples 100BDC0NDC-60, 75BDC25NDC-60, and 50BDC50NDC-60 exhibit higher specific surface area than respective samples 100BDC0NDC, 75BDC25NDC 50BDC50NDC, which were obtained without BA. The values were estimated as 1442, 1319 and 1195 m^2/g for the samples 100BDC0NDC-60, 75BDC25NDC-60, and 50BDC50NDC-60, respectively. It indicates the possible formation of defect pores. We have compared pore size distribution calculated according to the adsorption branches of isotherms for pairs of samples 100BDC0NDC/100BDC0NDC-60, 75BDC25NDC-60/75BDC25NDC-60, and 50BDC50NDC/50BDC50NDC-60. Samples obtained without BA additive demonstrated only regular pores about 6.3 and 7.4 Å (Fig.S 3 SI). Samples 100BDC0NDC-60, 75BDC25NDC-60, and 50BDC50NDC-60, along with these regular pores, contained larger defect cavities. So, FTIR and nitrogen adsorption data proved the formation of defect pores in samples synthesized with BA.

Fig. 4a represents the optical absorption spectra, which were tested via UV–Vis spectroscopy. The main absorption bands of UiO-66 are placed at 290–320 nm according to the type of linkers. They could be associated with ligand-to-metal charge transfer (LMCT). As expected, the functional groups' existence in an aromatic ring sharply influences the material optical properties. Absorption edges of UiO-66 are shifted from 450 to 300 nm with different linkers. The increase in NDC linker leads to a decrease in these edges and displays a blue shift compared to other samples (Table 2). As a result, the energy gap decreases with increasing NDC content from 4 eV to 3 eV, as demonstrated in Fig. 4b.

3.2. Photocatalytic performance

Before the photocatalytic tests, pure MB solution was irradiated with white light to make sure it was stable. We have not observed any significant changes in the UV–Vis-spectra of the solution (SI Fig.S 4). All synthesized samples have demonstrated photocatalytic activity in MB degradation (Fig. 5). Irradiation with light enhances MB degradation with MOFs (SI Fig.S 5). However, even in the dark, we have observed partial decolorization of MB solution. The increase in NDC content has led to the higher photocatalytic activity for samples with NDC-linker (0BDC100NDC, 50BDC50NDC, 75BDC25NDC). Such properties were previously reported for MOFs with naphthalene groups in linkers [30,40,41]. However, the 100BDC0NDC sample has exhibited photocatalytic activity as well.

We have considered three possible processes. The first one is the adsorption of MB into the cavities of MOFs. For UiO-66, this process was previously reported [6,32]. An increase in NDC content leads to a decrease in available pore volume. So, if adsorption dominates the process, a higher specific surface area should lead to a more effective decolorization of MB solutions. However, sample 0BDC100NDC with lower porosity has exhibited a higher rate of MB decolorization than 100BDC0NDC one. It could be attributed to possible stacking interactions between NDC-linker and MB molecules. It was reported that MB molecules could form dimers via π-π-interactions of the conjugated system of three benzene rings [42,43]. We suppose that naphthalene species of NDC-linker could attract MB molecules as well, resulting in fast and specific adsorption. We have observed that light irradiation strongly affects the decolorization of MB solution. In this way, we propose a two-step process: MOF samples adsorb MB molecules with subsequent photocatalytic degradation via NDC-linker in MOFs. We have observed that an increase in NDC content leads to a decrease in the bandgap (Table 2). It facilitates the excitation of electrons from valence to conductive band under light irradiation [44]. Such active particles could produce hydroxyl radicals, which possess high catalytic activity in dye degradation [40]. For zirconium-based MOF with 2,6-naphthalene dicarboxylate linker, a ligand-to-cluster charge transfer was investigated using the femtosecond transient absorption technique [45]. We have applied an additional experiment to specify which active particles are responsible for the decolorization process. Three additives were used in the photocatalytic process with a 0BDC100NDC sample: tret-butyl alcohol as a scavenger for OH-radicals, potassium dichromate for

Table 2
Characterization of the samples with various linker compositions. SSA stands for specific surface area, K designates reaction rate constant, MB removal was calculated after 30 min of mixing.

Samples designation	Space group (№)	a, Å	SSA, m [2]/g	K × 10^{-3} (min^{-1})	Energy gap, eV	MB removal, %	
						dark	light
100BDC0NDC	F m-3m (225)	20.75298	1159	41	3.32	44.0	77.25
75BDC25NDC		20.77295	1022	18	3.16	17.8	46.39
50BDC50NDC		20.79310	787	59	3.08	36.9	83.82
0BDC100NDC		20.85181	514	196	3.00	61.7	99.49

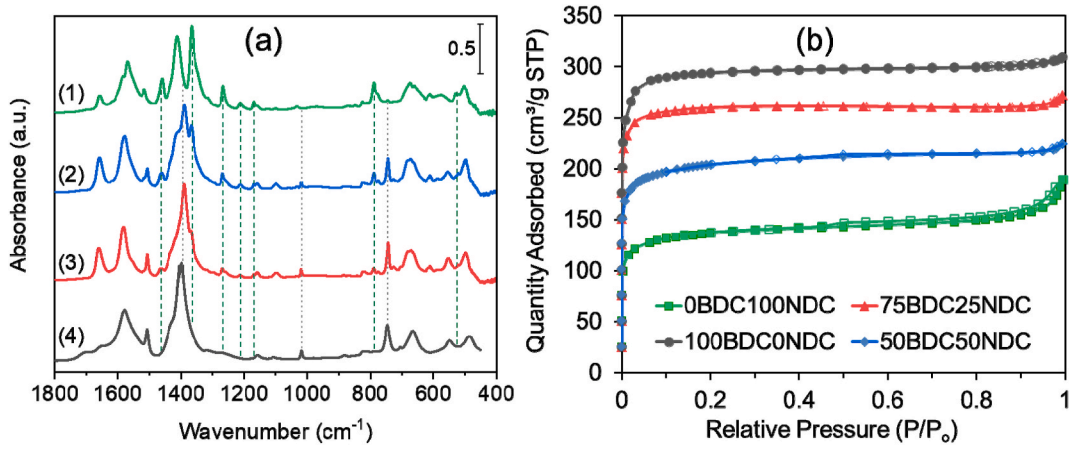

Fig. 2. (a) FTIR spectra of synthesized samples 0BDC100NDC (1), 50BDC50NDC (2), 75BDC25NDC (3), 100BDC0NDC (4). (b) Sorption isotherms of synthesized samples. Adsorption branches of isotherms are marked with filled symbols, while empty markers represent desorption branches.

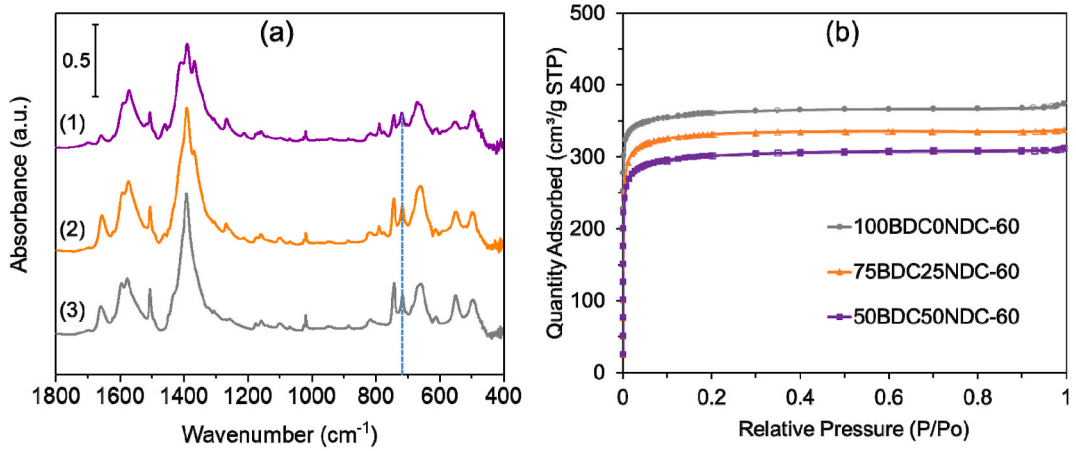

Fig. 3. (a) FTIR spectra of synthesized samples 100BDC0NDC-60, 75BDC25NDC-60 and 50BDC50NDC-60. Spectra were shifted along the y-axis for better representation. (b) Sorption isotherms of synthesized samples 100BDC0NDC-60, 75BDC25NDC-60 and 50BDC50NDC-60. Adsorption branches of isotherms are marked with filled symbols, while empty markers represent desorption branches.

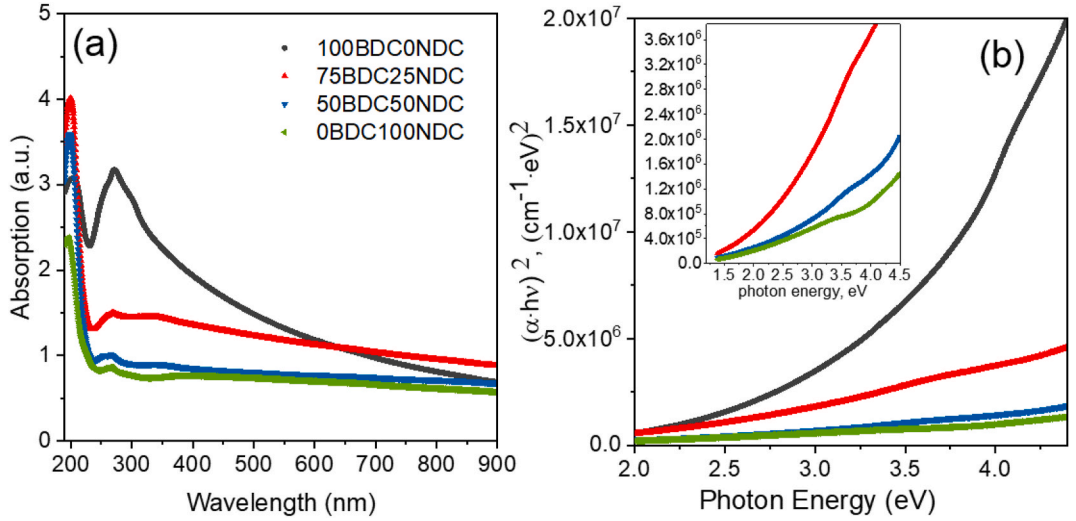

Fig. 4. UV–vis absorption spectra of 0BDC100NDC, 50BDC50NDC, 75BDC25NDC and 100BDC0NDC.

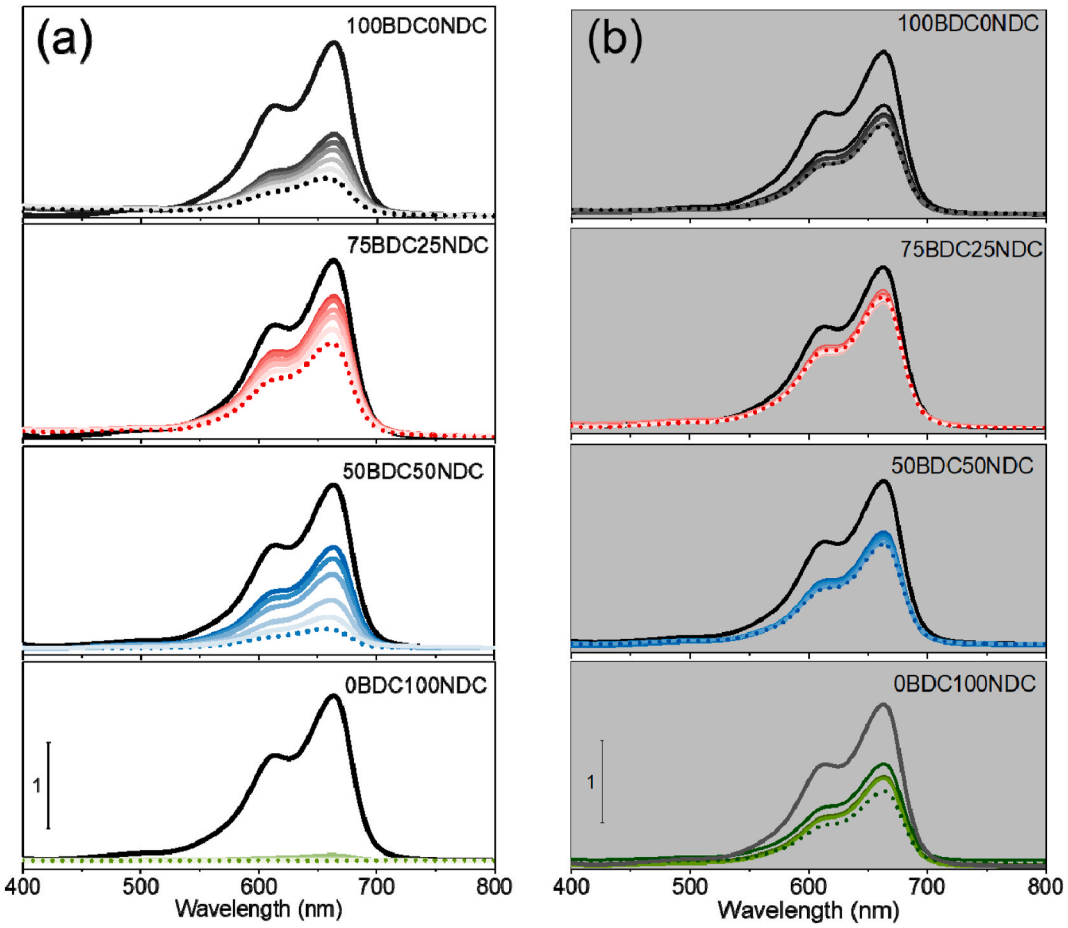

Fig. 5. The photocatalyst performance of synthesized samples under visible light irradiation (a) and dark (b). The black spectrum was measured from the MB solution used for the experiment. Dotted spectrum highlights solution after 30 min of the experiment.

electrons, and ammonium oxalate for holes. We have observed that tret-butyl alcohol twice decreased the efficiency of the photocatalytic MB degradation (SI Fig.S 6). Therefore, it proves that the formation of hydroxyl radicals causes the photocatalytic degradation of MB with synthesized MOFs. The estimated reaction rate constant is provided in Table 2 (see also SI Fig.S 7).

According to XRD, interaction with MB has not resulted in any significant changes in the crystal structure of MOF samples (Fig. 6a). FTIR spectra of MOF samples before and after interaction with MB solution are presented in Fig. 6b. As it could be observed, the 100BDC0NDC sample exhibited the most pronounced changes. Shoulder at 1550 cm^{-1} could be attributed to vibrations of the C-S-C group of MB molecules [43]. The broad region at 1320-1340 cm^{-1} is assigned to stretching vibrations of the C-N bond in dimethylamino groups and C=S

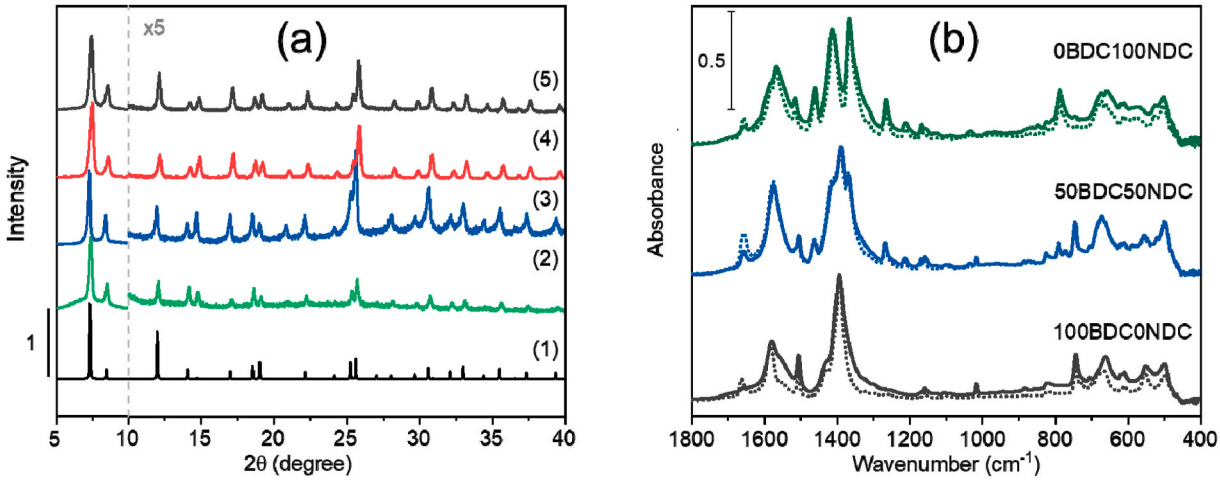

Fig. 6. (a) XRD powder patterns of samples 0BDC100NDC(2), 50BDC50NDC(3), 75BDC25NDC (4) and 100BDC0NDC (5). Black profile was calculated for the structure of UiO-66-NDC according to crystallographic data CCDC 1553924. (b) FTIR spectra of samples before (dotted lines) and after (solid lines) incubation in MB solution under light for 30 min.

vibrations of MB molecules [43]. We also suppose that contribution of C-S-C vibrations of MB results in a red-shift of the peak at 665 cm^{-1}. According to these observations, we could conclude that the 100BDC0NDC sample adsorbed more MB than samples 50BDC50NDC and 0BDC100NDC. It is in good agreement with high specific surface area and the largest pores of the 100BDC0NDC sample. Summarizing the effect of NDC-linker, we could propose the following decolorization process. Firstly, MOFs adsorb MB molecules, and this process occurs both in the dark and under light. Higher porosity should increase the dye removal according to adsorption. The second step is MB photocatalytic degradation under the visible light. NDC-linker boost ligand-to cluster charge transfer and enhance photocatalytic performance of the MOF. However, NDC-rings decrease specific surface area and pore aperture in the MOF. It results in non-linear trends in dye removal efficiency for 0BDC100NDC, 50BDC50NDC, 75BDC25NDC samples (Fig.S 5 SI).

It should be noted that not only NDC-linkers could have photocatalytic properties. Zirconium unsaturated sites in defect pores are also known to be active catalytic centers [46,47]. We have performed an additional experiment to evaluate the effect of unsaturated zirconium cites on MB degradation. Samples 100BDC0NDC-60, 50BDC50NDC-60, and 75BDC25NDC-60 with high defect concentration have been tested for the same reaction. We have observed that high defect concentration results in a high rate of MB degradation (Fig. 7). Moreover, we have revealed a shift of peaks for these samples. UV–Vis spectrum of MB solution contains two groups of characteristic peaks: at 664 and 610 nm corresponds to the sulfur-nitrogen conjugated system, while two peaks at 247 and 290 nm are assigned to phenothiazine structure. For the samples with low-defect concentration, we have observed a decrease in the intensity of these peaks without any shift (Fig. 7a, c, e). We have attributed it to the adsorption process with subsequent photocatalytic decomposition with the formation of mineral products. Samples with high defect concentration exhibited different behavior. Peaks at 290 and 247 nm have almost vanished in all samples even without light irradiation (Fig. 7b, d, f). It indicates oxidative decomposition of MB molecules with ring-opening reactions of the phenothiazine group. Moreover, we have observed that instead of two peaks at 664 and 610 nm spectra of MB solution after interaction with high-defect MOFs contained only one.

Fig. 8 represents spectra from Fig. 7 (for samples 50BDC50NDC/50BDC50NDC-60 and 100BDC0NDC/100BDC0NDC-60) with normalized intensities. It could be observed that sample 50BDC50NDC-60 has initiated a shift of peak in the spectrum of MB solution to 630 nm, sample 100BDC0NDC-60 to 620 nm. Contrary, 50BDC50NDC and 100BDC0NDC samples have caused changes only in peak intensity, not in their position. Such shifts could be attributed to the products of MB decomposition in the reaction mixture. It was reported that a peak at 630 nm could be attributed to Azure A (Fig. 8d), and a one at 620 nm could be assigned to Azure C (Fig. 8e). These products indicate oxidative demethylation as a possible pathway of MB degradation in the case of high defect samples. The high catalytic activity of unsaturated zirconium in defect sited was deep investigated [36,46–49].

FTIR spectra of 50BDC50NDC-60 and 100BDC0NDC-60 powders after MB removal are presented in Fig. 9. In good agreement with Azure C composition, the spectrum of 100BDC0NDC-60 sample does not contain a shoulder at 1340 cm^{-1} attributed to dimethylamino groups.

4. Conclusions

In the present work, UiO-66 derivates were applied as new photocatalysts for MB degradation. We have obtained a list of MOFs with two kinds of linkers in one phase: BDC and NDC. It allowed us to trace the effect of naphthalene rings' conjugated π-system on the photocatalytic process. We have observed a non-linear trend of MB removal, which corresponds to the complex process. The MB removal could be divided into two steps. The first step is the adsorption of the dye into the porous structure of MOF. The second step is photocatalytic degradation. NDC-linkers decrease available pore volume and therefore obstruct the first adsorption step. On the other hand, naphthalene rings take part in charge transfer processes, resulting in a decrease of bandgap and better photocatalytic properties. These two opposite trends lead to a decline in dye removal via MOF with low NDC content. The best performance showed a 0BDC100NDC sample, which removed 99 % of MB for 30 min. We also investigated the effect of unsaturated zirconium sites in defect pores on MB degradation. All defect samples exhibited high photocatalytic activity under visible light irradiation. Moreover, using FTIR and UV–Vis spectra, we have evaluated products of MB decomposition – Azure A and Azure C. It indicates that active zirconium sites alternate the degradation process and catalyze oxidative demethylation of MB. Obtained results show, that linker modification with naphthalene rings and the introduction of defects into the UiO-66 material enhance its photocatalytic properties. It leads to effective MB removal under visible

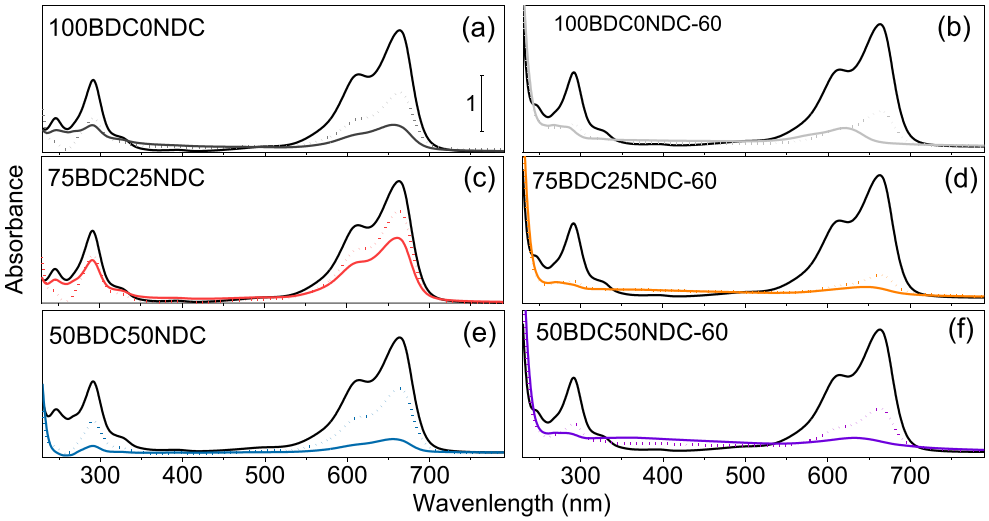

Fig. 7. The photocatalyst performance of samples 100BDC0NDC (a), 100BDC0NDC-60 (b), 75BDC25NDC (c), 75BDC25NDC-60 (d), 50BDC50NDC(e), and 50BDC50NDC-60 (f). Solid lines represent spectra measured from experiments with light irradiation, while dotted lines show spectra measured from experiments in darkness.

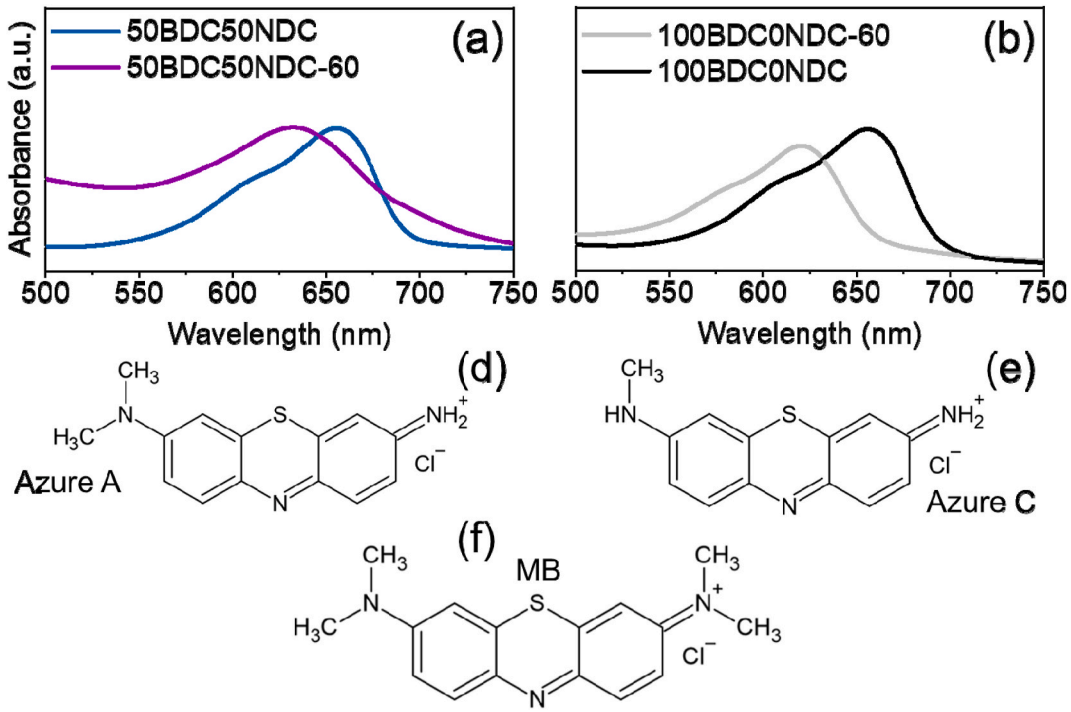

Fig. 8. UV–Vis spectra of MB solution after light irradiation with samples 50BDC50NDC and 50BDC50NDC-60 (a), 100BDC0NDC and 100BDC0NDC-60 (b). Intensities of peaks were normalized for better representation. (d)-(f) structural formulas of MB (f) and possible products of its decomposition: Azure A (d) and Azure C (e).

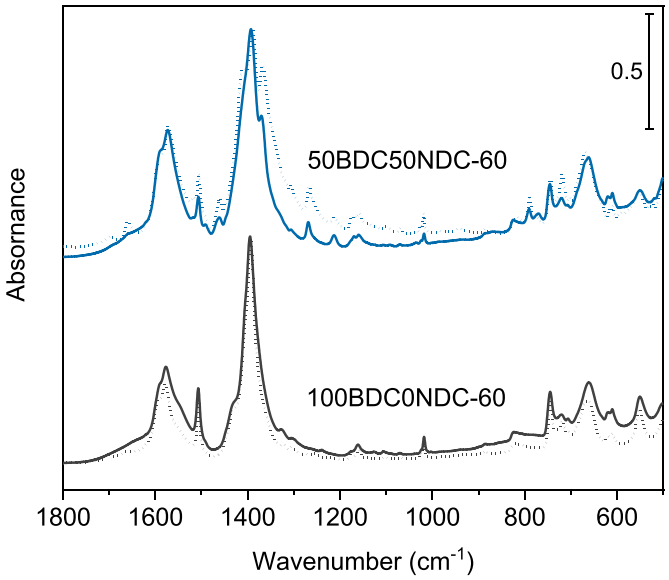

Fig. 9. FTIR spectra of samples 50BDC50NDC-60 and 100BDC0NDC-60 before (dotted lines) and after (solid lines) MB removal under light irradiation.

light irradiation.

CRediT authorship contribution statement

Vera V. Butova: Conceptualization, Methodology, Writing – review & editing, Visualization. **Abdelaziz M. Aboraia:** Writing – original draft, Formal analysis. **Malak Solayman:** Formal analysis, Investigation, Validation. **I.S. Yahia:** Resources, Project administration. **Heba Y. Zahran:** Resources. **Alaa F. Abd El-Rehim:** Investigation. **Hamed Algarni:** Investigation. **Gomaa Khabiri:** Formal analysis. **Alexander V. Soldatov:** Supervision, Resources.

Declaration of competing interest

The authors declare that they have no known competing financial interests or personal relationships that could have appeared to influence the work reported in this paper.

Acknowledgments

The authors express their appreciation to the Deanship of Scientific Research at King Khalid University for funding this work through a research groups program under grant number R.G.P.2/43/40. Aboraia and AVS acknowledge RFBR for financial support according to project No 19-32-90214.

Appendix A. Supplementary data

Supplementary data to this article can be found online at https://doi.org/10.1016/j.micromeso.2021.111314.

References

[1] X. Weng, Q. Zeng, Y. Zhang, F. Dong, Z. Wu, Facile approach for the syntheses of ultrafine TiO2 nanocrystallites with defects and C heterojunction for photocatalytic water splitting, ACS Sustain. Chem. Eng. 4 (2016) 4314–4320, https://doi.org/10.1021/acssuschemeng.6b00828.
[2] Q. Shen, et al., Hollow MnOx-CeO2 mixed oxides as highly efficient catalysts in NO oxidation, Chem. Eng. J. 322 (2017) 46–55, https://doi.org/10.1016/j.cej.2017.02.148.
[3] X. Zhang, et al., Study of catalytic activity at the Ag/Al-SBA-15 catalysts for CO oxidation and selective CO oxidation, Chem. Eng. J. 283 (2016) 1097–1107, https://doi.org/10.1016/j.cej.2015.08.064.
[4] X. Zhang, et al., Facile synthesis of new efficient Cu/MnO2 catalysts from used battery for CO oxidation, J. Environ. Chem. Eng. 5 (2017) 5179–5186, https://doi.org/10.1016/j.jece.2017.09.059.
[5] H. Pan, et al., Sphere-shaped Mn3O4 catalyst with remarkable low-temperature activity for methyl–ethyl–ketone combustion, Environ. Sci. Technol. 51 (2017) 6288–6297, https://doi.org/10.1021/acs.est.7b00136.

[6] Y. Wang, X. Li, G. Lu, G. Chen, Y. Chen, Synthesis and photo-catalytic degradation property of nanostructured-ZnO with different morphology, Mater. Lett. 62 (2008) 2359–2362, https://doi.org/10.1016/j.matlet.2007.12.019.

[7] Y.F. Wang, N. Ma, Orderings a class of unicyclic graphs with respect to Hosoya and Merrifield-Simmons index, Sains Malays. 45 (2016) 55–58.

[8] M. Sohail, et al., Synthesis of well-dispersed TiO2@reduced graphene oxide (rGO) nanocomposites and their photocatalytic properties, Mater. Res. Bull. 90 (2017) 125–130, https://doi.org/10.1016/j.materresbull.2017.02.025.

[9] S. Kumar, B. Ahmed, A.K. Ojha, J. Das, A. Kumar, Facile synthesis of CdO nanorods and exploiting its properties towards supercapacitor electrode materials and low power UV irradiation driven photocatalysis against methylene blue dye, Mater. Res. Bull. 90 (2017) 224–231, https://doi.org/10.1016/j.materresbull.2017.02.044.

[10] Saruchi, M. Sharma, M.R. Hatshan, V. Kumar, A. Rana, Sequestration of eosin dye by magnesium (II)-Doped zinc oxide nanoparticles: its kinetic, isotherm, and thermodynamic studies, J. Chem. Eng. Data 66 (2021) 646–657, https://doi.org/10.1021/acs.jced.0c00810.

[11] Saruchi, P. Thakur, V. Kumar, Kinetics and thermodynamic studies for removal of methylene blue dye by biosynthesize copper oxide nanoparticles and its antibacterial activity, J. Environ. Health Sci. Eng. 17 (2019) 367–376, https://doi.org/10.1007/s40201-019-00354-1.

[12] Saruchi, R. Verma, V. Kumar, A.A. Alothman, Comparison between removal of Ethidium bromide and eosin by synthesized manganese (II) doped zinc (II) sulphide nanoparticles: kinetic, isotherms and thermodynamic studies, J. Environ. Health Sci. Eng. 18 (2020) 1175–1187, https://doi.org/10.1007/s40201-020-00536-2.

[13] X. Zhang, et al., Effects of Ag loading on structural and photocatalytic properties of flower-like ZnO microspheres, Appl. Surf. Sci. 391 (2017) 476–483, https://doi.org/10.1016/j.apsusc.2016.06.109.

[14] Y. Yang, et al., Facile synthesis of ZnO/Ag nanocomposites with enhanced photocatalytic properties under visible light, Mater. Lett. 180 (2016) 97–100, https://doi.org/10.1016/j.matlet.2016.05.117.

[15] X. Zou, Y. Dong, X. Zhang, Y. Cui, Synthesize and characterize of Ag 3 VO 4/TiO 2 nanorods photocatalysts and its photocatalytic activity under visible light irradiation, Appl. Surf. Sci. 366 (2016) 173–180, https://doi.org/10.1016/j.apsusc.2016.01.034.

[16] J. Ethiraj, et al., Solvent-Driven gate opening in MOF-76-Ce: effect on CO2 adsorption, Chemsuschem 9 (2016) 713–719, https://doi.org/10.1002/cssc.201501574.

[17] L.H. Wee, et al., 1D-2D-3D transformation synthesis of hierarchical metal-organic framework adsorbent for multicomponent alkane separation, J. Am. Chem. Soc. 139 (2017) 819–828, https://doi.org/10.1021/jacs.6b10768.

[18] A.L. Bugaev, et al., Operando study of palladium nanoparticles inside UiO-67 MOF for catalytic hydrogenation of hydrocarbons, Faraday Discuss 208 (2018) 287–306, https://doi.org/10.1039/c7fd00224f.

[19] V.V. Butova, et al., The effect of cobalt content in Zn/Co-ZIF-8 on iodine capping properties, Inorg. Chim. Acta. 492 (2019) 18–22, https://doi.org/10.1016/j.ica.2019.04.011.

[20] K.S. Vetlitsyna-Novikova, V.V. Butova, I.A. Pankin, V.V. Shapovalov, A. V. Soldatov, Zirconium-based metal-organic UiO-66, UiO-66-NDC and MOF-801 frameworks. Influence of the linker effect on the hydrogen sorption efficiency, J. Surf. Investig. 13 (2019) 787–792, https://doi.org/10.1134/s1027451019050173.

[21] V.V. Butova, et al., Modification of ZIF-8 with triethylamine molecules for enhanced iodine and bromine adsorption, Inorg. Chim. Acta. 509 (2020) 5, https://doi.org/10.1016/j.ica.2020.119678.

[22] I.E. Gorban, et al., L-leucine loading and release in MIL-100 nanoparticles, Int. J. Mol. Sci. 21 (2020) 11, https://doi.org/10.3390/ijms21249758.

[23] V.V. Butova, I.A. Pankin, O.A. Burachevskaya, K.S. Vetlitsyna-Novikova, A. V. Soldatov, New fast synthesis of MOF-801 for water and hydrogen storage: modulator effect and recycling options, Inorg. Chim. Acta. 514 (2021) 7, https://doi.org/10.1016/j.ica.2020.120025.

[24] Y. Gao, S. Li, Y. Li, L. Yao, H. Zhang, Accelerated photocatalytic degradation of organic pollutant over metal-organic framework MIL-53(Fe) under visible LED light mediated by persulfate, Appl. Catal. B Environ. 202 (2017) 165–174, https://doi.org/10.1016/j.apcatb.2016.09.005.

[25] L. Shi, et al., An amine-functionalized iron(III) metal–organic framework as efficient visible-light photocatalyst for Cr(VI) reduction, Adv. Sci. 2 (2015), https://doi.org/10.1002/advs.201500006.

[26] Y. Pan, et al., A new Zn(ii)-based 3D metal-organic framework with uncommon sev topology and its photocatalytic properties for the degradation of organic dyes, CrystEngComm 21 (2019) 4578–4585, https://doi.org/10.1039/c9ce00759h.

[27] Z.C. Hao, S.C. Wang, Y.J. Yang, G.H. Cui, Syntheses, structural diversities and photocatalytic properties of three nickel(II) coordination polymers based semi-bis (benzimidazole) and aromatic dicarboxylic acid ligands, Polyhedron 181 (2020), https://doi.org/10.1016/j.poly.2020.114466.

[28] F.J. Zhao, G.L. Zhang, Z.F. Ju, Y.X. Tan, D.Q. Yuan, The combination of charge and energy transfer processes in MOFs for efficient photocatalytic oxidative coupling of amines, Inorg. Chem. 59 (2020) 3297–3303, https://doi.org/10.1021/acs.inorgchem.9b03743.

[29] Y. Xia, K.X. Wang, J.S. Chen, Synthesis, structure characterization and photocatalytic properties of two new uranyl naphthalene-dicarboxylate coordination polymer compounds, Inorg. Chem. Commun. 13 (2010) 1542–1547, https://doi.org/10.1016/j.inoche.2010.09.008.

[30] S. Pu, L. Xu, L. Sun, H.B. Du, Tuning the optical properties of the zirconium-UiO-66 metal-organic framework for photocatalytic degradation of methyl orange, Inorg. Chem. Commun. 52 (2015) 50–52, https://doi.org/10.1016/j.inoche.2014.12.015.

[31] Q. Chen, et al., Selective adsorption of cationic dyes by UiO-66-NH2, Appl. Surf. Sci. 327 (2015) 77–85, https://doi.org/10.1016/j.apsusc.2014.11.103.

[32] A.A. Mohammadi, et al., Metal-organic framework Uio-66 for adsorption of methylene blue dye from aqueous solutions, Int. J. Environ. Sci. Technol. 14 (2017) 1959–1968, https://doi.org/10.1007/s13762-017-1289-z.

[33] J.H. Qiu, Y. Feng, X.F. Zhang, M.M. Jia, J.F. Yao, Acid-promoted synthesis of UiO-66 for highly selective adsorption of anionic dyes: adsorption performance and mechanisms, J. Colloid Interface Sci. 499 (2017) 151–158, https://doi.org/10.1016/j.jcis.2017.03.101.

[34] H. Molavi, A. Hakimian, A. Shojaei, M. Raeiszadeh, Selective dye adsorption by highly water stable metal-organic framework: long term stability analysis in aqueous media, Appl. Surf. Sci. 445 (2018) 424–436, https://doi.org/10.1016/j.apsusc.2018.03.189.

[35] D. Yang, et al., Tuning the surface chemistry of metal organic framework nodes: Proton topology of the metal-oxide-like Zr6 nodes of UiO-66 and NU-1000, J. Am. Chem. Soc. 138 (2016) 15189–15196, https://doi.org/10.1021/jacs.6b08273.

[36] M. Vandichel, et al., Active site engineering in UiO-66 type metal-organic frameworks by intentional creation of defects: a theoretical rationalization, CrystEngComm 17 (2015) 395–406, https://doi.org/10.1039/c4ce01672f.

[37] V.V. Butova, et al., Partial and complete substitution of the 1,4-benzenedicarboxylate linker in UiO-66 with 1,4-naphthalenedicarboxylate: synthesis, characterization, and H 2 -adsorption properties, Inorg. Chem. 58 (2019) 1607–1620, https://doi.org/10.1021/acs.inorgchem.8b03087.

[38] V.V. Butova, et al., UiO-66 type MOFs with mixed-linkers - 1,4-Benzenedicarboxylate and 1,4-naphthalenedicarboxylate: effect of the modulator and post-synthetic exchange, Microporous Mesoporous Mater. 305 (2020), 110324, https://doi.org/10.1016/j.micromeso.2020.110324.

[39] Z.G. Pei, et al., Adsorption characteristics of 1,2,4-trichlorobenzene, 2,4,6-trichlorophenol, 2-naphthol and naphthalene on graphene and graphene oxide, Carbon 51 (2013) 156–163, https://doi.org/10.1016/j.carbon.2012.08.024.

[40] M. Dai, et al., Three zinc(II) coordination polymers based on tetrakis(4-pyridyl) cyclobutane and naphthalenedicarboxylate linkers: solvothermal syntheses, structures, and photocatalytic properties, Cryst. Growth Des. 14 (2014) 240–248, https://doi.org/10.1021/cg4014416.

[41] Y. Gong, T. Wu, J. Lin, Metal–organic frameworks based on naphthalene-1,5-diyldioxy-di-acetate: structures, topologies, photoluminescence and photocatalytic properties, CrystEngComm 14 (2012) 3727–3736, https://doi.org/10.1039/C2CE06529K.

[42] K. Bergmann, C.T. O'Konski, A spectroscopic study OF methylene blue monomer, dimer, and complexes with montmorillonite, J. Phys. Chem. 67 (1963) 2169–2177, https://doi.org/10.1021/j100804a048.

[43] O.V. Ovchinnikov, et al., Manifestation of intermolecular interactions in FTIR spectra of methylene blue molecules, Vib. Spectrosc. 86 (2016) 181–189, https://doi.org/10.1016/j.vibspec.2016.06.016.

[44] A. Wang, et al., Titanium incorporated with UiO-66(Zr)-type metal–organic framework (MOF) for photocatalytic application, RSC Adv. 6 (2016) 3671–3679, https://doi.org/10.1039/C5RA24135A.

[45] M. Gutierrez, B. Cohen, F. Sánchez, A. Douhal, Photochemistry of Zr-based MOFs: ligand-to-cluster charge transfer, energy transfer and excimer formation, what else is there? Phys. Chem. Chem. Phys. 18 (2016) 27761–27774, https://doi.org/10.1039/C6CP03791G.

[46] P. Ponchai, et al., Engineering zirconium-based UiO-66 for effective chemical conversion of D-xylose to lactic acid in aqueous condition, Chem. Commun. 56 (2020) 8019–8022, https://doi.org/10.1039/d0cc03424j.

[47] W.L. Xiang, et al., The metal-organic framework UiO-66 with missing-linker defects: a highly active catalyst for carbon dioxide cycloaddition, Appl. Energy 277 (2020), https://doi.org/10.1016/j.apenergy.2020.115560.

[48] C.M. Granadeiro, et al., Production of ultra-deep sulfur-free diesels using a sustainable catalytic system based on UiO-66(Zr), Chem. Commun. 51 (2015) 13818–13821, https://doi.org/10.1039/C5CC03958D.

[49] A. Dhakshinamoorthy, A. Santiago-Portillo, A.M. Asiri, H. Garcia, Engineering UiO-66 metal organic framework for heterogeneous catalysis, ChemCatChem 11 (2019) 899–923, https://doi.org/10.1002/cctc.201801452.